Effects of in-cylinder flow simplifications on turbulent mixing at varying injection timings in a piston bowl ppc engine

Ibron, Christian; Jangi, Mehdi; Bai, Xue Song

DOI:
10.4271/2019-01-0220

No number

Effect of injection timing on the ignition and mode of combustion in a HD PPC engine running low load

Christian Ibron, Mehdi Jangi,Sara Lonn, Alexios Matamis, Oivind Andersson, Martin Tuner, Mattias Richter, Xue-Song Bai
Lund Institute of Technology, Sweden

ABSTRACT

This work aims to study the effect of fuel inhomogeneity on the ignition process and subsequent combustion in a compression ignition Partially Premixed Combustion (PPC) engine using a *Primary reference Fuel* (PRF) in low load conditions. Five cases with injection timings ranging from the *start of injection* (SOI) at -70 crank angle degrees (CAD) to -17 CAD have been studied numerically and experimentally in a heavy duty (HD) piston bowl geometry. Intake temperature is adjusted to to keep the combustion phasing constant. Three dimensional numerical simulations are performed in a closed cycle sector domain using the Reynolds Averaged Navier-Stokes (RANS) formulation with k-ϵ turbulence closure and direct coupling of finite rate chemistry. The results are compared with engine experiments. The predicted trends in required intake temperature and auto-ignition location for a constant combustion phasing are consistent with experiments. The simulations show that the auto-ignition is critically dependent on both fuel and temperature stratification. The ignition occurs in fuel-lean regions but the mixing of the fuel with the cylinder gas and the cylinder gas temperature stratification (prior to injection) determines the ignition location. A higher heat release rate is observed in the later injection cases, which is attributed to the higher equivalence ratio of the mixture inside the bowl. Negative temperature coefficient (NTC) heat release behaviour of the studied fuel plays a role in shortening the ignition wave propagation but the impact of the effect varies among the injection cases. A sensitivity study of combustion efficiency with regard to the intake temperature is performed on two of the cases (SOI of -30 CAD and of -63 CAD). While the combustion phasing is slower and correctly predicted in the simulations of the advanced injection cases the combustion efficiency is found to be very sensitive to the intake temperature. This is attributed to the high sensitivity of the ignition delay time to equivalence ratio and temperature.

INTRODUCTION

As an alternative to existing engine concepts, PPC engines have been shown to achieve very high indicated mean efficiencies in laboratory conditions while retaining low level of particulate matter (PM) and nitric oxides (NO_x) [8, 10]. PPC is part of a branch of concepts in the community of combustion engine research which are often referred to as low temperature combustion (LTC) concepts. A common theme for these concepts is that the rate of combustion is controlled by attaining a stratification in ignition delay times. This is typically done by making the fuel burn at least partially in a lean environment, lowering the combustion temperature. The PPC combustion concept is achieved by injecting the fuel into the cylinder in such a way as to create a stratification in the fuel gas concentration, higher than in the homogeneous charge compression ignition (HCCI) concept but lower than in conventional diesel combustion (CDC). The diluted fuel/oxidizer mixture is then ignited by compression ignition which allows for high compression ratios. The reactivity spreads in the cylinder through an ignition wave front which is propagating due to increasing cylinder temperature caused by the mechanical compression and by the pressure rise due to combustion. The reduction of NO_x and PM is caused by the leaner combustion environment which generally means cooler combustion. The potential increase in efficiency of PPC engines compared to diesel is often accredited to the reduced heat losses that result from said cooler combustion event [15].

While the high efficiencies of PPC engines have been experimentally verified the difficulties to control the combustion phasing has been hindering the concept from operating in the same wide range of conditions as CDC. Meth-

ods for controlling the phasing in various fuel types such as diesel [4], gasoline [7, 3] and alcohol fuels [17] have been studied. Control parameters include injection timing, exhaust gas recirculation (EGR) and intake temperature amongst others [18, 16]. From a modeling point of view the the challenge lies in correctly describing the reactivity which differs from both CDC and SI engines. The oxidation in a PPC engines happens in a mix of combustion modes with the ignition wave front dominating the early combustion [23, 24]. The spontaneous ignition of nonuniform premixed fuel/oxidizer mixtures has been studied by Zel'dovich [22] who showed that the combustion mode changes between ignition wave front and deflagration wave, depending on the stratification of ignition delay time (IDT). The balance of ignition wave front propagation to deflagration in non-uniform mixtures of a blend of high and low reactivity fuels have been studied by Bhagatwala et al and Kim et al. [1, 9]. These studies show that depending on conditions both fuel and temperature fluctuations can slow down the reaction front due to a higher amount of deflagration wave mode. The in-cylinder fluctuations of fuel and temperature in PPC engines vary with injection timing, intake temperature and level of compression. This makes the study of the coupling between said factors an important topic for PPC engines.

Experimentally the effect of injection timing on the combustion process for a single injection has been studied by Li et al. [12] in a heavy duty single cylinder metal engine and Lonn et al. [14] in an optical quartz piston engine. Both studies reported that the required intake temperature to keep the combustion phasing constant varied non-monotonically with SOI timing, which was speculated to be due to both injection timing and the injector/piston bowl geometric effects. Lonn additionally provided radial position of ignition kernels for said SOI's. The aim of this work is to identify mechanisms/recurring phenomena in the ignition process and subsequent combustion and to validate the simulation setup for a wide span of the T_{IVC} parameter. The study is limited to cases of fixed CA50 which is controlled by variation in T_{IVC} for all cases.

METHODOLOGY AND SETUP

NUMERICAL SETUP The engine conditions being studied correspond to a low load case of the opetical experiments of Lonn et al. [14] with no EGR and a medium swirl ratio of 2.2. The engine is modified based on the Scania D13 diesel engine. Table 1 describes the general engine conditions for all the studied cases and Table 2 shows case-wise injection information. Five different cases of fuel, oxidizer and temperature distributions at the moment of injection are studied by varying the SOI in the range -70 CAD ATDC to -17 CAD ATDC. These injection timings are spread out so that the spray impingement location varies from liner to piston bowl in order to observe the range of fuel stratification due to the spray/liner and spray/bowl interaction (cf. figure 1). CFD model is used simulate the flow, injection, mixing and combustion in a single cylinder in the compression and earlier expansion stroke, from IVC until 30 CAD ATDC. The pressure at IVC is chosen so that the in-cylinder pressure without combustion follows a so-called hot motored case (recorded pressure from a skip-fire cycle) from the experiments. Additionally, the IVC cylinder gas temperature T_{IVC} is chosen such that half of the fuel energy is released at a prescribed crank-angle (CA50). In the simulation T_{IVC} is varied for each case individually to match up the prescribed CA50, and then in-cylinder pressure trace and the first ignition sites from the simulations are compared with the experiments. This has the thermodynamic implication that the mass of the cylinder gas varies slightly between cases and this in turn shifts the global equivalence ratio slightly from case to case. Since the simulation starts at the moment of intake valve closing the flow field from the gas exchange is approximated by a solid body rotation flow with spatially uniform turbulent kinetic energy, turbulent dissipation rate and temperature.

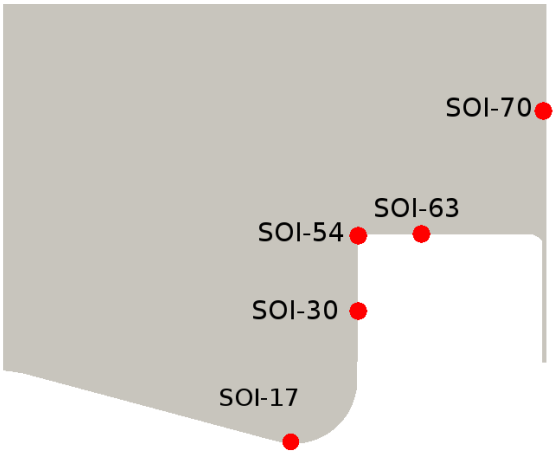

Figure 1: Cross section of the cylinder showing a central plane of the sector mesh. Approximate spray impingement locations after half injection duration for all injection cases are marked with red dots.

Table 1: Details of the simulation case based on the Scania D13 optical engine cylinder experiments of Lonn et al. [14].

Detail	Value
Bore	130 mm
Squish	1.2 mm
Connecting rod	255 mm
Compression ratio	14.1
Engine speed	1200 rpm
IVC	-160 CAD ATDC
Swirl number	2.2
Domain sector angle	45 deg
Oxygen level (vol.)	21 %
Fuel	PRF 81
Fuel mass (single nozzle)	5.56 mg
Constant CA50	4.5 CAD aTDC
Global eq. ratio λ	3.5 - 3.7

ENGINE GEOMETRY, GRID AND NUMERICS The simulation geometry is based on a single optical Scania

Table 2: Actual SOI for the cases and the cylinder back pressure at the beginning of said SOI.

Case	SOI [CAD ATDC]	Back pressure [bar]
SOI-17	-16	28.1
SOI-30	-29	15.9
SOI-54	-53	6.3
SOI-63	-62	4.8
SOI-70	-69	3.8

D13 heavy duty cylinder with quartz piston studied in Lonn et al. [14]. No part of the gas exchange cycle is included in the simulation, the cylinder head geometry is flat and the optical quartz piston has no valve pockets. The flow is resolved in a mesh made of exclusively hexahedral cells with cell counts varying between 700 000 cells and 200 000 cells depending on which injection timing is studied. All cells have a Jacobian determinant value of at least 0.5 at all times. The typical cell side length in radial and axial dimensions is roughly 0.5 mm but the tangential mesh size varies from 0.1 mm to 1.5 mm due to the nature of a sector mesh with O-grid. A small radius of the sector center (0.5 mm) is cut away and replaced with a symmetry boundary conditions to avoid high aspect ratio tetrahedral cells. Topology displacement is handled by uniform translation of cell nodes in the piston axis direction with flux compensation. Because of this the cell aspect ratio is changing with time - to maintain cell quality the mesh was changed at -20 CAD ATDC for cases with injections from SOI of -54 CAD ATDC and earlier. Spatial discretization are all Gaussian integration linear type with second order accuracy. The simulation utilizes adjustable time-step control, keeping the CFL number below 0.15.

PHYSICS MODELING

Turbulence The simulations are performed in the open source software OpenFOAM with a custom solver developed at Lund University. For simulating the fluid motion the model utilizes the RANS formulation of the Navier-Stokes equations with the standard $\mathrm{k}-\epsilon$ turbulence model which models turbulent transport by introducing a turbulent eddy viscosity. The standard $\mathrm{k}-\epsilon$ coefficients are used. It is important to keep in mind that the RANS result corresponds to that of an ensemble average of infinite number of engine cycles. Turbulent kinetic energy, turbulent dissipation rate and heat conductivity close to the walls are modeled by wall functions.

Spray Fuel spray is modeled using the stochastic Lagrangian particle tracking method. The breakup of the droplets is handled by the standard Kelvin-Helmholtz/Rayleigh-Taylor model implemented in OpenFOAM[20, 5]. The simulation utilizes a droplet dispersion model which couples the transported subgrid turbulent kinetic energy to the momentum direction of the newly formed droplets. The injection liquid mass flow rate

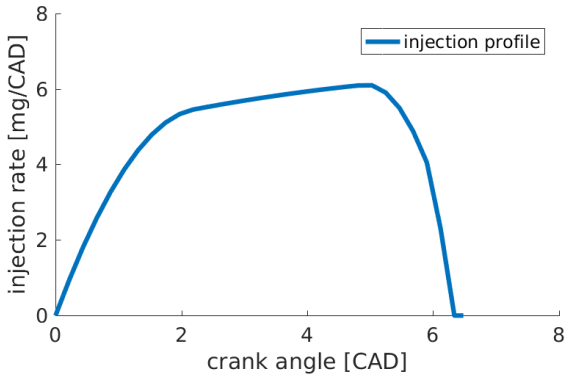

Figure 2: The figure depicts the injection profile of the spray. This profile was obtained from Xu et al. [21].

profile was predicted using a recently developed injection model [21]. Figure 2 shows the injection mass flow rate profile from the model. The discharge coefficient was set to 0.9 for all cases. The size of the droplet introduced at the nozzle hole is set by a Weibull distribution with an average Sauter mean diameter (SMD) of 60 μm and a k-value of 3. The droplets are introduced at saturated liquid temperature and can only interact with the flow and the walls i.e. no droplet-droplet interaction. Testing showed that spray behavior converged when using at least 50 000 parcels.

Chemistry A simplified PRF chemical mechanism consisting of 44 species and 140 reactions is used to represent the chemistry [13]. The mass fraction of each species is transported in an Eulerian field and reacts according to the Arrhenius coefficients of the chemical mechanism. The solver utilizes chemistry coordinate mapping for chemistry speedup as described by Jangi et al. [6]. The well stirred model (WSR) is used and therefore turbulence exerts no influence on the mean reaction rates in each computational cell. This is justified by the fact that in PPC engine the combustion starts with ignition (where chemical reactions occur in wide regions and thus less sensitive to the turbulence/chemistry interaction), and ends with diffusion controlled combustion (which is dictated by the turbulence mixing rate and thus less sensitive to the mean reaction rates). This is in contrast to spark-ignition engine combustion where chemical reactions occur in thin layers and flame/turbulence interaction dictates the combustion process.

SPRAY VALIDATION

The sweep of injection timings covers a wider range of cylinder gas conditions and it is interesting to examine whether a single set of spray model constants could replicate the spray characteristics of all of these cases. In order to validate the spray model natural luminosity Mie scattering images published by Lonn et al. [14] are compared with spray simulations under evapora-

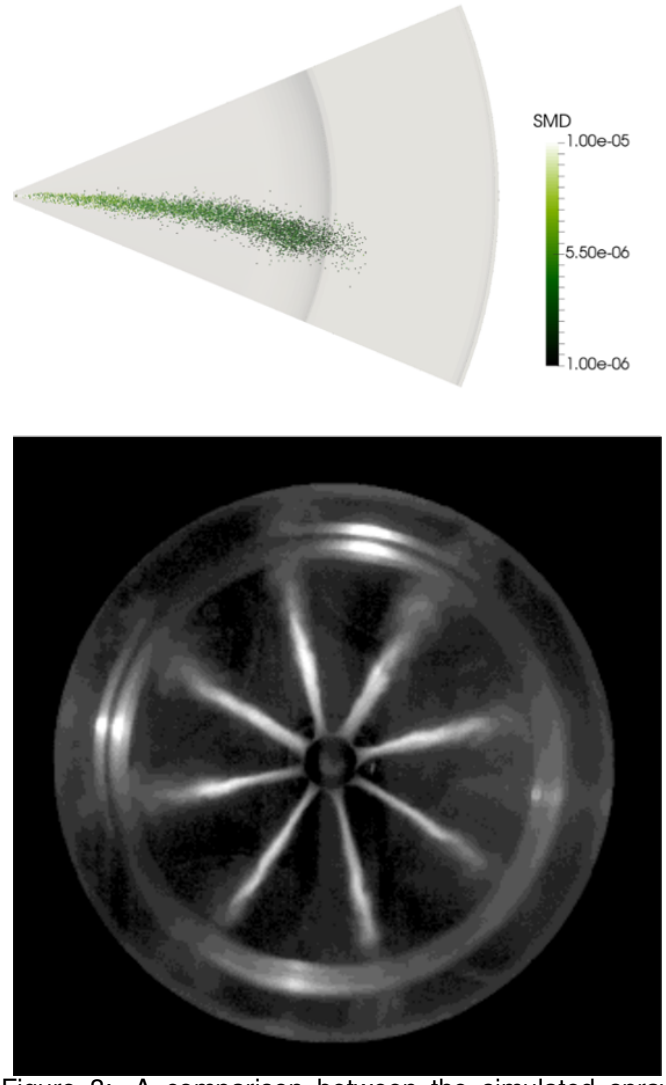

Figure 3: A comparison between the simulated spray parcels and Mie scattering spray image by Lonn et al. [14] for the case SOI -54 CAD ATDC. The experimental picture (lower) shows the piston bowl and a small strip of the squish region. As can be seen, the smallest visible droplets are transported by the swirl before evaporating. The spray model break-up timescale coefficient B1 is adjusted to 20, which is shown to replicate the spray characteristics from the experiments.

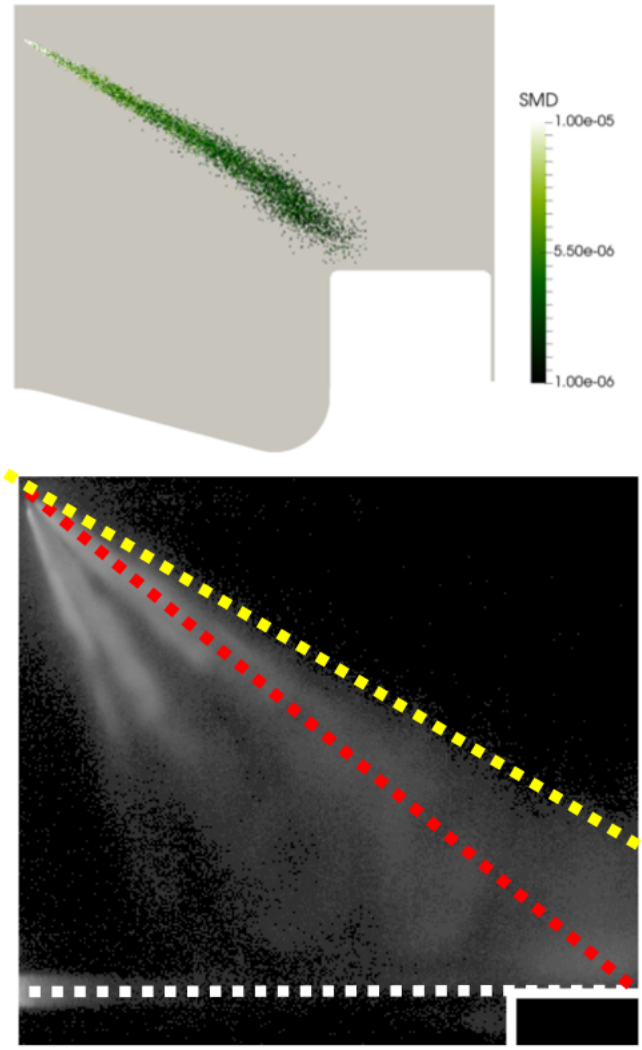

Figure 4: The bottom image is a Mie spray image by Lonn et al. [14] at roughly -52 CAD ATDC for the SOI-54 case. The white solid line indicates the piston shape. The dotted lines indicate spray center (red), outside spray cone (yellow) and squish level (white). The image is not corrected for distortion. The upper image shows the spray distribution and Sauter mean diameter of the Lagrangian parcels in the spray model. The spray model break-up timescale coefficient B1 is adjusted to 20, which is shown to replicate the spray characteristics from the experiments. The impingement position of the spray is dependent on the penetration speed.

tion conditions (but without combustion). While the signal intensity is not comparable between images and nonlinear to droplet size it is still a good indication on the spread of the droplets and the liquid penetration of the spray. In the simulations the initial droplet size distribution was kept the same for all cases as well. The only model parameter that was adjust to replicate the spray images is the breakup timescale coefficient B1 in the KHRT model. It is found that B1 of 20 gives the best prediction of the spray liquid penetration for all cases listed in Table 2. This value of B1 is consistent with the value reported in the literature (where B1 has been reported to vary from originally stated 10 up to 40 [5, 20]). Figures 3 and 4 show the droplets distribution from the simulations for the SOI-54 case and the corresponding Mie scattering images. The simulated liquid penetration in both figures are in qualitatively good agreement with the Mie scattering images. The effect of swirl on the droplet distribution at the spray tip is clearly evidenced in the simulations and (to a low degree) also in the Mie scattering images.

IGNITION IDENTIFICATION The onset of local ignition is defined in this work as a heat release rate reaching $5 \cdot 10^9$ Joules per second and cubic meter, which is less than 1% of the peak heat release rate. This definition enables the identification of the multiple ignition locations in the cylinder. When multiple ignition kernels are detected within 1 crank angle they count as a single ignition event, even if they are separated spatially.

RESULTS AND DISCUSSION

Figure 5 shows a comparison of the in-cylinder pressure from the CFD simulations and experiments [14]. In the simulations T_{IVC} was adjusted to match up the same combustion phasing as in the experiments (with CA50 at 4.5 CAD ATDC). The overall agreement between the experiments and simulations is fairly good; however, the peak pressure is over-predicted for the earlier injection cases (SOI-70) and the later injection cases (SOI-30 and SOI-17). This is to certain extent due to the uncertainties in the experimentally reported amount of fuel injected, which may vary from cases to cases. In the simulations the injected fuel mass has been kept the same for all cases, which may not be the case in the experiments. Despite this difference it is noted that the shape of the pressure curves and thus the pressure rise rate at different CADs from the simulations are consistent with the experiments. In particular, both the simulations and experiments show an increase of the peak pressure rise rate as the injection is delayed, which reflects the fact that the combustion process in the studied cases is different, as analyzed in the following.

To understand the combustion process, the flow structure, the mixing field, and the earlier ignition event are examined. Figure 6 shows some of the key flow and scalar quantities at the instance of time of the high temperature ignition.

SOI-17 In this case the spray impinges on the deepest point of the piston bowl, cf. Fig. 1. The fuel is mixed with the surrounding gas in the bowl at a fast pace in the spray shear layer and impingement induced turbulence. As shown in Fig. 6e the fuel is mainly distributed inside the bowl. At the instance of time of the onset of high temperature ignition (1 CAD ATDC), most fuel is in the mixture with an equivalence ratio of 0.6 to 1, cf. Fig. 7. Once ignited the heat release rate is high owing to the close-to-stoichiometry mixture. This is believed to be the main reason that the pressure rise rate of this later injection case is the highest among all studied cases. In the region near the bowl wall the local equivalence ratio is close to 1 and the temperature is about 600K. One can see high concentration of ketohydroperoxide (C7KET) in the low temperature near-wall region. C7KET is an indicator species of low temperature reaction [19]. It has been observed that before the onset of high temperature ignition (for brevity the figure is not shown here), a large fraction of the fuel goes through the low temperature ignition reactions and a small amount of heat is released when C7KET is oxidized. This is known as the first-stage ignition, or sometimes referred to as the cool flame. The heat release from the cool flame results in increased temperature of the mixture, which implies that the required T_{IVC} would be lower if the heat release from the cool flame is higher. Furthermore, the competition of high temperature ignition chemistry and low temperature ignition chemistry affects the ignition delay time in an non-monotonic way [19], which is known as negative temperature coefficient (NTC): within the NTC regime, a lower initial temperature gives rise to a shorter ignition delay time. With NTC, given a certain equivalence ratio, the ignition wave propagation can be faster, since

$$V_{ig}^{-1} = \nabla \tau_{ig}(x) = \frac{d\tau_{ig}(T(x))}{dT} \nabla T(x) \qquad (1)$$

where V_{ig} is the speed of the ignition wave, τ_{ig} is the ignition delay time (which is a function of temperature and equivalence ratio). With NTC the value of $d\tau_{ig}/dT$ is lower and as such V_{ig} is higher. NTC could be one of the reasons of the high pressure rise rate of the later injection cases since in these cases the mixture is fuel-richer and relative colder than the early injection cases; thus, the NTC behavior is more significant in the later injection cases.

SOI-30 For the SOI-30 case the fuel is injected into the the piston bowl hitting the vertical piston bowl wall. The fuel travels along the floor of the bowl and is mixed with the surrounding gases at a high rate due to the strong spray induced turbulence. Some fuel is transported to the squish region; however most fuel is inside the bowl. Prior to any significant heat release low temperature ignition reactions take place first in the very lean regions around the spray, moving through the bulk of the fuel at -13 CAD ATDC. It is clear that at the onset of high temperature ignition some C7KET can still be observed near the piston bowl wall, which is similar to the later injection

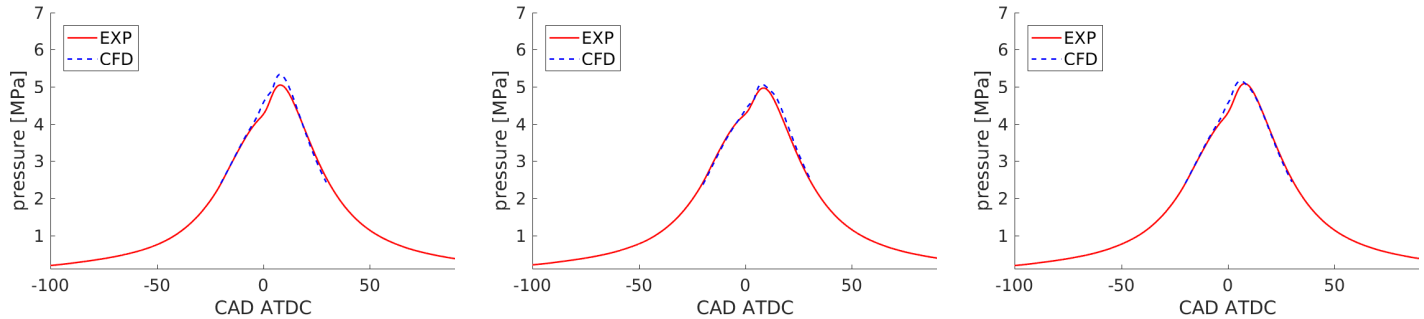

(a) SOI-70 (b) SOI-63 (c) SOI-54

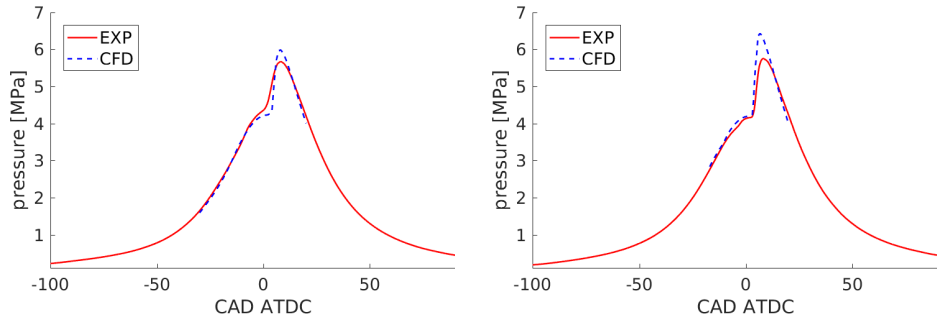

(d) SOI-30 (e) SOI-17

Figure 5: A comparison between the simulated and ensemble average experimental pressure traces for all five cases.

case SOI-17 discussed earlier. Owing to the 13 CAD earlier injection (than case SOI-17), the fuel/air mixture at the onset of ignition is better mixed, with equivalence ratio ranging from 0.5 to 0.75, leaner than the case SOI-17. Thus, once ignited, the total heat release rate is slightly lower and the pressure rise rate is also slightly lower than that in the SOI-17 case. The effect of NTC chemistry is also less intense than in the SOI-17 case, which can also slow down the ignition wave propagation (thus heat release rate). The main ignition starts deep inside the piston bowl at an equivalence ratio around 0.6, and the high temperature ignition becomes significant at 2 CAD ATDC.

SOI-54 In this case, the fuel spray impinges close to the piston lip (Fig. 1) and the fuel stream is split into two roughly equal fuel clouds forming in the squish and bowl regions. Roughly 2.5% of the total injected fuel hits the liner and enters into the crevice. Low temperature ignition reactions starts at -25 CAD ATDC in both clouds, and at the onset of high temperature ignition some C7KET can be observed in the squish region and also in the thin layer very close to the bowl wall, Fig. 6. Both clouds have equivalence ratios around 0.4 (cf. Fig. 7), which is the reason that the heat release rate and pressure rise rate is lower once it is ignited. Due to stronger wall interaction the cloud in the squish region has a lower temperature than the bowl cloud which makes the first ignition event appear in the bowl cloud at -2 CAD ATDC. An ignition wave propagates through the bowl cloud until the average in-cylinder pressure peaks at 6 CA ATDC. Thereafter, the compression heat is just high enough to ignite the squish cloud. This sequential ignition process in the bowl and in the squish room gives rise to the slower heat release rate and pressure rise rate shown in Fig. 5.

SOI-63 In this case, the spray impinges on the squish region (Fig. 1) and the fuel moves along the the squish, a part of it entering the crevice. The crevice fuel mass is estimated to be 5% of the total injected amount. The fuel in the crevice is not fully oxidized, which is one of the reasons of the lowest peak pressure for this case among all cases studied. Low temperature reactions start at -20 CAD ATDC. The fuel cloud is transported into the bowl region by the squish flow and at the onset of high temperature ignition the mixture has a local equivalence ratio around 0.3 to 0.4. At -1.5 CAD ATDC the mixture is ignited in the bowl region near the piston lip at an equivalence ratio of 0.35 and the combustion spreads through the squish in an ignition wave front until 8 CAD ATDC. Around this time the peak cylinder pressure is reached but still a significant amount of the fuel in the squish region is not combusted. This contributes further to the lower peak pressure. Thereafter, the fuel/air mixture in the squish region is oxidized in the combustion mode of premixed flame

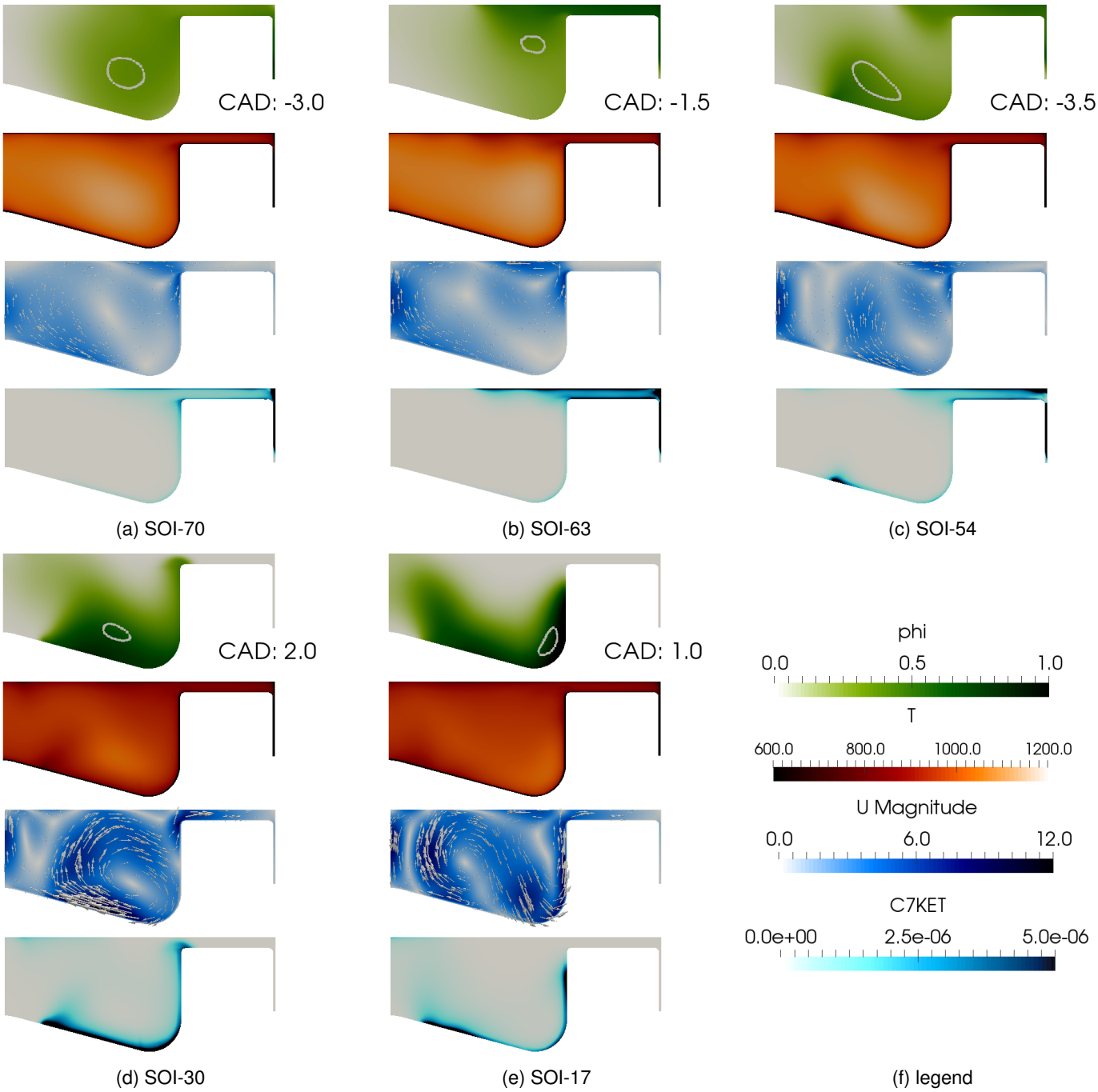

Figure 6: The equivalence ratio, temperature, surface projected velocity distribution and ketohydroperoxide (C7KET) mass fraction over the central cross section of the sector at the start of ignition for all cases. The ring in the equivalence ratio indicates the region at which the volumetric heat release rate is $5 \cdot 10^9 J/(m^3 \cdot s)$.

propagation, which is the reason of the slower heat release rate and pressure rise rate in this case. A double heat release rate peak is visible in this case due to the dual combustion modes (to be shown below).

SOI-70 In this case the fuel spray impinges on the liner (Fig. 1), creating a fuel cloud above the squish region which spreads into the bowl during the compression stroke. Low temperature ignition reactions start at -25 CAD ATDC but the mixture is so lean (local equivalence ratio around 0.3) that heat release rate is low. Just prior to the high temperature ignition which occurs at -3 CAD ATDC the fuel is spread into most of the piston and has a near uniform distribution. Due to the low concentration gradient and low temperature gradient in this case, the heat release rate is slightly higher than the case SOI-63. The amount of fuel in the squish region is lower than the case of SOI-63, which indicates the two-stage combustion process in the case of SOI-63 is less significant in the SOI-70 case.

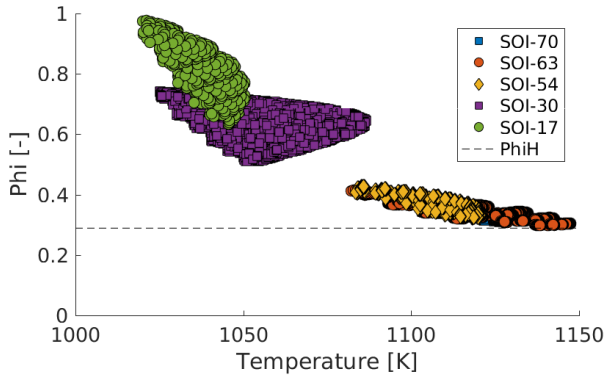

Figure 7: Scatter plot of cells with heat release rates higher than $5 \cdot 9^{10} J/(m^3 s)$ at the saved time step closest to ignition (at most 0.5 CA). The warmest cells in each case can be approximated as points on a line of constant ignition delay time. The value of $\frac{\delta\phi}{\delta T}$ on the line increases as the mixture gets leaner. The dotted line is the equivalence ratio of a fully homogeneous mixture.

INTAKE TEMPERATURE SENSITIVITY STUDY The cases SOI-30 and SOI-63 were used to investigate the sensitivity of the combustion and ignition to the initial cylinder gas temperature, T_{IVC}. The resulting pressure traces and heat release graphs can be seen in figures 8 and 9.

SOI-30 sensitivity For the range of T_{IVC} studied, a general trend can be observed: (a) The pressure rise rate of all CFD cases is higher than the experiments. This is believed to be due to the smoothed temperature and fuel distribution in the cylinder predicted by the RANS model. In reality, small-scale spatial variation of temperature and concentration exists, which slows down the combustion and heat release process, resulting a lower pressure rise rate. (b) With increasing T_{IVC} the heat release rate is higher, the ignition starts earlier and the total heat release is more complete. This shows the high sensitivity of the combustion to the initial temperature of the charge. With 15 K difference of T_{IVC} the studied cases have shown a change of CA50 about 7 CAD. For all of the cases studied the majority of the heat release happens prior to the peak cylinder pressure, Fig. 8. The single peak heat release rate profile indicates that the combustion process in this case is mainly governed by the ignition wave propagation.

SOI-63 sensitivity For this case the heat release rate is slower than the later injection case (the SOI-30 case) and the CFD pressure rise rate is in better agreement with the experiments with T_{IVC} of 430 K, Fig. 9. With earlier injection the mixture is more homogeneous in space and RANS can capture the mixing and subsequently the combustion process better (than for the later injection cases, SOI-17 and SOI-30). The T_{IVC} has been varied for 30 K. For this range of T_{IVC} the combustion process varies from complete combustion to nearly misfire (with only 10% heat released for the case T_{IVC} of 410K). The heat release rate profile shows two peaks owing to the dual combustion modes discussed earlier. Such a staged combustion process due to the formation of two fuel clouds in the bowl and in the squish region makes an interesting case to study combustion slowing effects from multiple combustion modes.

DISCUSSION

Combustion heat release rate and sensitivity In order to understand the trends in required initial gas temperature and ignition location one must first consider the state of the fuel cloud at the onset of ignition, as depicted in figures 6 and 7. The direction and magnitude of the gradient of the ignition delay time in respect to fuel concentration $\frac{d}{d\phi}\tau_{ig}$ varies drastically in the operating range of the stated cases[2, 11]. Even though the early injections which ignite at very lean conditions will have a low stratification in fuel concentration the relatively small differences in equivalence ratio cause drastic differences in ignition delay time $\Delta\phi\frac{d}{d\phi}\tau_{ig}$, where $\Delta\phi$ is some characteristic fuel stratification. The slow combustion phasing of the early injections can be accredited to this phenomenon. This also implies that a small error in the simulated turbulent transport of the fuel causes a big error in combustion modeling. The late injections at the other hand are igniting in richer regions which smaller and comparable values of $\Delta\phi\frac{d}{d\phi}\tau_{ig}$ and $\Delta T\frac{d}{dT}\tau_{ig}$ (with ΔT being some characteristic measure of temperature stratification). For these cases the stratification of ignition delay time will be smaller which results in a quicker combustion. The Reynolds averaged fields for temperature and fuel concentration underestimate the stratification of the ignition delay time, and because there is no mechanism present to compensate for unresolved (turbulent) transport and reaction the combustion speed is too high.

Inlet temperature The combustion phasing is controlled by means of the inlet temperature in the experiment and the initial temperature of the charge T_{IVC} in the numerical simulations. Figure 10 shows these temperatures. In general, the trend of the inlet temperature in the experiments and T_{IVC} in the numerical simulations with respect to the variations of SOI is consistent. The values of these temperatures are slightly different, with T_{IVC} being higher, due to the difference in the timing and location at which these temperatures are determined. Of particular interest one can point out that the required inlet temperatures and T_{IVC} is highest in the earlier injection cases, and lowest in the SOI-30 case. Such variation is a result of the dependence of the onset of ignition on the mixture temperature and equivalence ratio. For the current fuel/air mixtures, numerical simulations of ignition delay time in homogeneous mixtures shows that for a given temperature, mixtures with

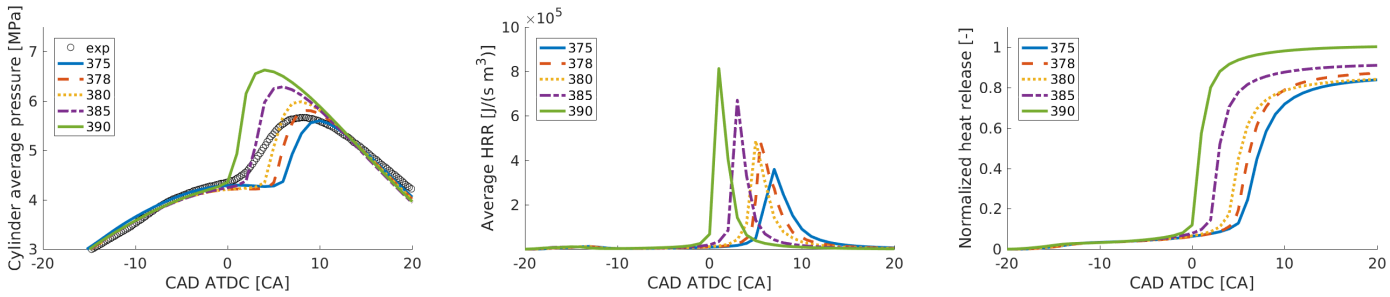

Figure 8: Effect of varying intake temperature on combustion for the SOI-30 case. From left to right: pressure traces, heat release rates and the accumulated heat release.

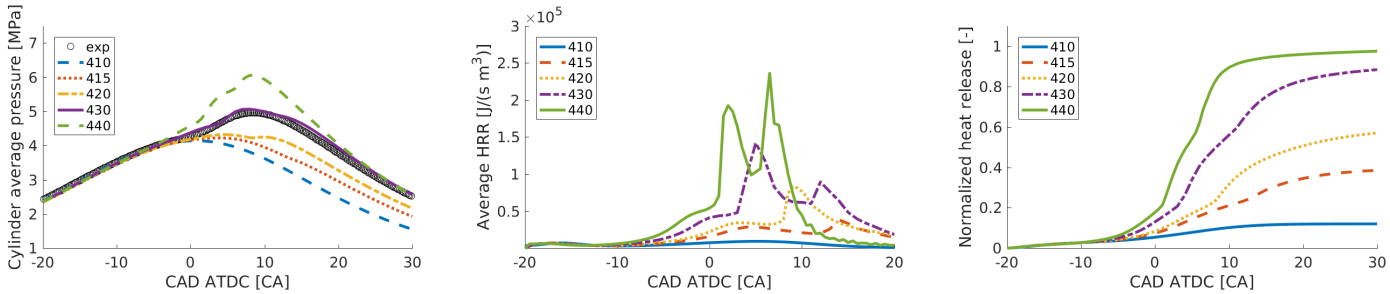

Figure 9: Effect of varying intake temperature on combustion for the SOI-63 case. From left to right: pressure traces, heat release rates and the accumulated heat release.

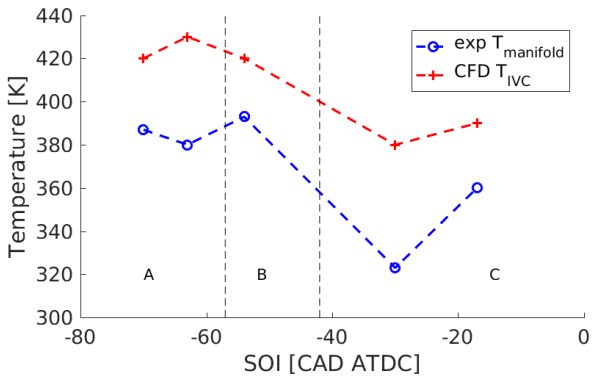

Figure 10: A comparison between the required T_{IVC} for constant CA50 in simulations and experiments. The regions A, B and C indicate that the spray hits outside the bowl, partially outside the bowl or entirely inside the bowl. The experimental trend is replicated but with an offset. This could be explained in part by the difference in the time and location of the intake thermal sensor measurement was done and T_{IVC} was determined.

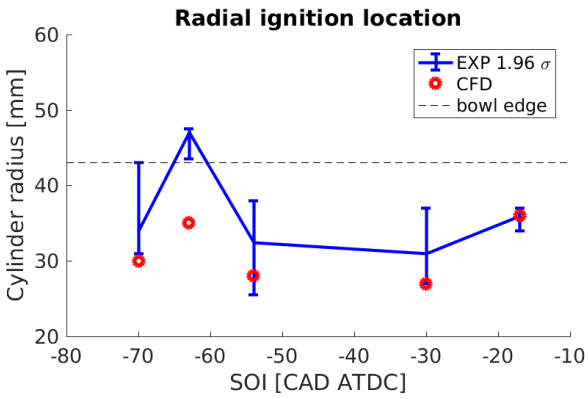

Figure 11: A comparison of radial ignition location between the experimental values based on luminosity and the simulation results based on heat release rate. The nonlinear behavior is captured by the simulations.

higher equivalence ratio have shorter ignition delay time. In another word, to achieve a constant ignition delay time, a fuel-leaner mixture requires higher initial temperature. This explains the general trend of the required high inlet temperature in the earlier injection cases, since the earlier injection cases have longer time to achieve more homogeneous mixing and thus fuel-leaner mixture, cf. Fig. 7. For the late injection case SOI-17 the required intake temperature rises again because the reduction in ignition delay time caused by richness is now offset by an increase in ignition delay time caused by low temperature. The break-point in ignition delay time reduction caused by fuel richness and high temperature seems to be around the conditions found in the SOI-30 case, which is implied by it having the lowest required intake temperature.

Ignition location The location of the first ignition sites are marked in Fig. 6 using the white circle. Figure 11 shows the respective radial distance of these ignition sites from the experiments and simulations. The dashed line indicates the radial position of the piston bowl edge. The overall trend of the ignition location from the simulations is consistent with the experiments. As seen in Fig. 6 the ignition location in the SOI-63 case is close to the squish region since most of the fuel in the squish region due to the particular injection timing and impingement location of the spray. The radial position shown in the experiments indicates that first ignition site is in the squish region outside the bowl whereas in the numerical simulation it is near the edge of the bowl, very close to the squish region. In all other cases, the ignition occurs inside the bowl, rather close to the floor of the bowl. The predicted ignition location is in closer agreement with the experiments in the later injection cases. The first ignition sites are the places where mixture has the shortest ignition delay time. Furthermore, the ignition process is sensitive to the local flow, since high flow strain rate (high scalar dissipation rate) can give rise to high heat loss, which competes with the heat release from the ignition process and delays the ignition process.

CONCLUSIONS

CFD simulations of low load single cylinder PPC engine runing with PRF fuels are carried out to investigate the effect of injection timing on the PPC ignition and heat release process. The CFD results are compared with the optical engine experiments of Lonn et al. [14]. The main findings are summerized below.

- The CFD simulation with RANS models and LPT spray model can replicate the experimental results in terms of in-cylinder pressure, location of the ignition, and the required inlet temperature to achieve a constant combustion phasing (CA50).
- For the studied cases it is found that with early injection the mixture is more homogeneous and fuel-leaner, which requires high inlet temperature to achieve the same ignition timing as the later injection cases. In the later injection cases, on other hand, the fuel is mainly inside the bowl; the mixture has a higher local equivalence ratio, which requires a lower inlet temperature to achieve the same CA50 as the earlier injection cases.
- The combustion begins in ignition wave front mode for all the cases but changes to premixed flame mode in the early injection cases after peak pressure is reached. The heat release rate for the early injection cases is shown to be slow due to the existence of dual combustion mode. The richer mixture inside the bowl in the later injection cases also results in high heat release rate once ignited.
- The spray impingement location to the cylinder/bowl walls is shown to be influential to the ignition and combustion process. In intermediate injection timing (SOI of -54 CAD ATDC) it is found that the fuel is split into two clouds, one in the bowl and one in the squish region. This results in two ignition events, first in the bowl and then in the squish region. The combustion heat release is slower and the required inlet temperature is the higher. Such fuel split can be a useful measure to achieve staged combustion and slower pressure rise rate.

ACKNOWLEDGMENTS

This work was sponsored by the Swedish Research Council and Kompetenscenter för Förbränningsprocesser (the KCFP project) at Lund University. The CFD simulations were performed on resources provided by the Swedish National Infrastructure for Computing (SNIC) at PDC and HPC2N centers.

REFERENCES

[1] A. Bhagatwala, R. Sankaran, S. Kokjohn, and J. H. Chen, *Numerical investigation of spontaneous flame propagation under RCCI conditions*, Combustion and Flame, 162 (2015), pp. 3412–3426.

[2] S. S. Goldsborough, *A chemical kinetically based ignition delay correlation for iso-octane covering a wide range of conditions including the NTC region*, Combustion and Flame, 156 (2009), pp. 1248–1262.

[3] R. M. Hanson, S. L. Kokjohn, D. A. Splitter, and R. D. Reitz, *An Experimental Investigation of Fuel Reactivity Controlled PCCI Combustion in a Heavy-Duty Engine*, SAE International Journal of Engines, 3 (2010), pp. 2010–01.

[4] W. L. Hardy and R. D. Reitz, *A Study of the Effects of High EGR, High Equivalence Ratio, and Mixing Time on Emissions Levels in a Heavy-Duty Diesel Engine for PCCI Combustion*, in SAE 2006 World Congress & Exhibition, SAE International, 4 2006.

[5] C. HUANG AND A. LIPATNIKOV, *Modelling of Gasoline and Ethanol Hollow-Cone Sprays Using OpenFOAM*, 8 2011.

[6] M. JANGI AND X.-S. BAI, *Multidimensional chemistry coordinate mapping approach for combustion modelling with finite-rate chemistry*, Combustion Theory and Modelling, 16 (2012), pp. 1109–1132.

[7] G. T. KALGHATGI, P. RISBERG, AND H.-E. ÅNGSTRÖM, *Advantages of Fuels with High Resistance to Auto-ignition in Late-injection, Low-temperature, Compression Ignition Combustion*, SAE International, 3 2006.

[8] G. T. KALGHATGI, P. RISBERG, AND H.-E. NGSTRM, *Partially Pre-Mixed Auto-Ignition of Gasoline to Attain Low Smoke and Low NOx at High Load in a Compression Ignition Engine and Comparison with a Diesel Fuel*, SAE International, 3 2007.

[9] S. O. KIM, M. B. LUONG, J. H. CHEN, AND C. S. YOO, *A DNS study of the ignition of lean PRF/air mixtures with temperature inhomogeneities under high pressure and intermediate temperature*, Combustion and Flame, 162 (2015), pp. 717–726.

[10] S. KIMURA, O. AOKI, H. OGAWA, S. MURANAKA, AND Y. ENOMOTO, *New combustion concept for ultra clean and high efficiency small DI diesel engine.pdf*, in SAE Technical Paper 1999-01-3681, 1999.

[11] J. KODAVASAL AND S. SOM, *Gasoline Compression IgnitionA Simulation-Based Perspective*, Springer, Singapore, 2018, pp. 227–249.

[12] C. LI, P. TUNESTAL, M. TUNER, AND B. JOHANSSON, *Comparison of Gasoline and Primary Reference Fuel in the Transition from HCCI to PPC*, 10 2017.

[13] Y.-D. LIU, M. JIA, M.-Z. XIE, AND B. PANG, *Enhancement on a Skeletal Kinetic Model for Primary Reference Fuel Oxidation by Using a Semidecoupling Methodology*, Energy & Fuels, 26 (2012), pp. 7069–7083.

[14] S. LONN, A. MATAMIS, M. TUNER, M. RICHTER, AND O. ANDERSSON, *Optical Study of Fuel Spray Penetration and Initial Combustion Location under PPC Conditions*, 3 2017.

[15] V. MANENTE, *Gasoline Partially Premixed Combustion - An Advanced Internal Combustion Engine Concept Aimed to High Efficiency, Low Emissions and Low Acoustic Noise in the Whole Load Range*, PhD thesis, Lund University, 2010.

[16] V. MANENTE, B. JOHANSSON, P. TUNESTAL, AND W. J. CANNELLA, *Influence of Inlet Pressure, EGR, Combustion Phasing, Speed and Pilot Ratio on High Load Gasoline Partially Premixed Combustion*, 5 2010.

[17] V. MANENTE, P. TUNESTAL, B. JOHANSSON, AND W. J. CANNELLA, *Effects of Ethanol and Different Type of Gasoline Fuels on Partially Premixed Combustion from Low to High Load*, 4 2010.

[18] V. MANENTE, C.-G. ZANDER, B. JOHANSSON, P. TUNESTAL, AND W. CANNELLA, *An Advanced Internal Combustion Engine Concept for Low Emissions and High Efficiency from Idle to Max Load Using Gasoline Partially Premixed Combustion*, SAE International, 3 2010.

[19] N. PETERS, G. PACZKO, R. SEISER, AND K. SESHADRI, *Temperature cross-over and non-thermal runaway at two-stage ignition of n-heptane*, Combustion and Flame, 128 (2002), pp. 38–59.

[20] R. D. REITZ AND J. C. BEALE, *MODELING SPRAY ATOMIZATION WITH THE KELVIN-HELMHOLTZ/RAYLEIGH-TAYLOR HYBRID MODEL*, Atomization and Sprays, 9 (1999), pp. 623–650.

[21] L. XU, X.-S. BAI, M. JIA, Y. QIAN, X. QIAO, AND X. LU, *Experimental and modeling study of liquid fuel injection and combustion in diesel engines with a common rail injection system*, Applied Energy, 230 (2018), pp. 287–304.

[22] Y. ZELDOVICH, *Regime classification of an exothermic reaction with nonuniform initial conditions*, Combustion and Flame, 39 (1980), pp. 211–214.

[23] F. ZHANG, R. YU, AND X. BAI, *Direct numerical simulation of PRF70/air partially premixed combustion under IC engine conditions*, Proceedings of the Combustion Institute, 35 (2015), pp. 2975–2982.

[24] ——, *Effect of split fuel injection on heat release and pollutant emissions in partially premixed combustion of PRF70/air/EGR mixtures*, Applied Energy, 149 (2015), pp. 283–296.